incorporates the old idea by Emslie (1934) based on propagation of electrons along atom strings. HOLZ rings of circular shape are thus related to the repetition b along the zone axis – as would be the case for individual strings. The potential at the string, *cf.* (2), is interpreted as the potential $V(j)$ seen by a strongly excited Bloch wave. The resulting increment in wavelength is related to the (negative) increment in wave vector given by the eigenvalue $\gamma^{(j)}$ [(7)] through the kinetic energy. The circular rings correspond to Bloch waves with low potential energy, located near the atom strings, sometimes called 'tightly bound'. Bloch waves with higher potential energy will usually display more interference effects associated with interference between scattering in different strings and the typical HOLZ-line fine structure consisting of curved or straight Kikuchi- or Kossel-line segments. Our description is equivalent to the theory developed by Steeds & co-workers (Steeds, 1983).

The description is seen to apply to experimental patterns taken in reflection as well as in transmission and in intermediate configurations, including CBED patterns and channeling appearing in Kikuchi pattern and surface channeling.

We thank Professor J. M. Cowley for many valuable discussions. Part of the work was supported by NSF grant DMR-8510059 and made use of the resources of the ASU Facility for High Energy Electron Microscopy, supported by NSF grant DMR-8611609.

References

COWLEY, J. M. (1975). *Diffraction Physics.* Amsterdam: North-Holland.

EMSLIE, A. G. (1934). *Phys. Rev.* **45**, 43–46.

GJØNNES, J., HAFNOR, O. A. & HØIER, R. (1971). *Jernkontorets Ann.* **155**, 471–472.

KIKUCHI, S. & NISHIKAWA, S. (1928). *Proc. Imp. Acad. (Tokyo)*, **4**, 475.

PENG, L.-M. & COWLEY, J. M. (1988). *Surf. Sci.* **201**, 559–572.

PENG, L.-M., COWLEY, J. M. & YAO, N. (1988). *Ultramicroscopy*, **26**, 189–194

SHINOHARA, K. (1932). *Sci. Pap. Inst. Phys. Chem. Res. (Jpn)*, **20**, 39.

STEEDS, J. M. (1983). In *Quantitative Electron Microscopy*, edited by J. N. CHAPMAN & A. J. CRAVEN. Scottish Univ. Summer School in Physics, Edinburgh, Scotland.

TERASAKI, O., WATANABE, D. & GJØNNES, J. (1979). In Proc. Fifth Int. Conf. on High-Voltage Electron Microscopy, p. 263.

Acta Cryst. (1989). A**45**, 703–708

Determination of the Enantiomorph from Intensity Measurements of Three-Beam Bragg-Surface Diffraction of X-rays

BY SHIH-SEN CHIEN, MAU-TSU TANG AND SHIH-LIN CHANG*

Department of Physics, National Tsing-Hua University, Hsinchu, Taiwan 30043

(*Received* 27 *December* 1988; *accepted* 15 *May* 1989)

Abstract

An analytical expression for the intrinsic peak width of three-beam Bragg diffraction involving a surface reflection is derived on the basis of the dynamical theory of X-ray diffraction. Utilization of this expression in peak intensity measurements is proved to lead to direct determination of the enantiomorph of the triplet structure-factor invariant involved in a three-beam Bragg-surface diffraction. Effects of polarization on the kinematical peak intensity and on the intrinsic peak width are also discussed.

1. Introduction

The use of X-ray multiple diffraction for phase determination has long been proposed (Lipscomb, 1949). Investigations on the possibilities of extracting phase information from the intensity variation near or at the exact multi-beam diffraction position have been intensively pursued in recent years. These include the work reported by Hart & Lang (1961), Ewald & Héno (1968), Colella (1974), Post (1977), Jagodzinski (1980), Chapman, Yoder & Collella (1981), Chang (1981, 1982), Høier & Aanestad (1981), Juretschke (1982*a*, *b*), Hümmer & Billy (1982, 1986), Høier & Marthinsen (1983), Post, Nicolosi & Ladell (1984), Chang (1986, 1987), Shen (1986), Thorkildsen (1987), Mo, Haubach & Thorkildsen (1988), Shen & Colella (1988) and many others.

Recently, quantitative determination of the phases of structure-factor triplets using intensity profiles of three-beam (a primary, a secondary and an incident beam) diffraction has been demonstrated by Chang & Tang (1988) and Tang & Chang (1988). In that discussion, Bragg–Laue and Bragg–Bragg types of

* To whom all correspondence should be addressed.

0108-7673/89/100703-06$03.00

three-beam interaction were dealt with, where the former involved a primary reflection of Bragg type and a secondary reflection of Laue type; the latter involved only Bragg-type reflections. In addition, the enantiomorph associated with the signs of the (triplet) phases for noncentrosymmetric crystals [see, for example, Ladd & Palmer (1980)] is determined by the scaling procedure proposed. Alternatively, an experiment for the determination of the enantiomorph has also been reported very recently (Hümmer, Weckert & Bondza, 1989). The theoretical ground on which the experiment is based is given in the paper of Hümmer & Billy (1986). In a three-beam diffraction, when either the primary or the secondary reflection is of surface type (see Fig. 1), *i.e.* the corresponding wavevector is along the crystal surface, difficulties arise in the determination of the enantiomorph. It is the purpose of this paper to provide a way of overcoming these difficulties. Consequently, a method is proposed for determining the enantiomorph from the measurement of peak intensities of surface three-beam diffractions.

For convenience, we use in the following the term three-beam Bragg-surface diffraction to denote the case in which the primary reflection is a symmetric Bragg reflection and the secondary is a surface reflection.

2. Theoretical considerations

Consider a three-beam (O, G, L) diffraction, where O, G and L are the incident, the primary and the secondary reflections, respectively (see Fig. 1*a*). Assume that G is a symmetric Bragg reflection. Fig. 1(*a*) shows the geometry of the three-beam Bragg-surface case in reciprocal space, where the three reciprocal-lattice points O, G and L are on the surface of the Ewald sphere. The reciprocal-lattice vectors of the primary and secondary reflections are **g** and **l**, respectively. According to Chang & Tang (1988), the relative intensity distribution of the primary reflection G in the vicinity of the three-beam position can be written as a function of the azimuthal angle φ of rotation around the vector **g** as

$$I'_G = [I_G(3) - I_G(2)]/I_G(2) = I_d + I_k, \qquad (1)$$

where $I_G(3)$ and $I_G(2)$ are the diffraction intensities of the G reflection in the three- and two-beam positions, respectively. I_d and I_k are the dynamical and kinematical intensities defined as

$$I_d = 2Pa_1Q[2(\Delta\varphi)\cos\delta - \eta_i \sin\delta] \qquad (2)$$

$$I_k = a_2P^2 \qquad (3)$$

where

$$P = |\Gamma|k^2Q(|F_{G-L}||F_L|/|F_G|)/(2W) \qquad (4)$$

$$Q = [(\Delta\varphi)^2 + (\eta_i/2)^2]^{-1/2} \qquad (5)$$

$$\eta_i = G_2|\chi_0|/W \qquad (6)$$

$$W = kl \sin\alpha \sin\beta \cos\theta_G \qquad (7)$$

$$G_2 = k^2\gamma_L/\gamma_0. \qquad (8)$$

Γ is equal to $-r_e\lambda^2/\pi V$, where r_e is the classical radius of the electron. V and λ are the volume of the crystal unit cell and the wavelength used. F's are the structure factors, which are proportional to the electric susceptibilities $\chi/4\pi$ as $\chi = \Gamma F$. l is the modulus of the reciprocal-lattice vector **l**. η_i is the intrinsic peak width. θ_G is the Bragg angle of the G reflection. The angles α and β are defined in Fig. 1. γ_O and γ_L are the direction cosines of the O and the L reflected beams with respect to the inward crystal surface normal. $\Delta\varphi$ is the azimuthal angle measured from the exact three-beam diffraction position. a_1 and a_2 are the polarization factors which were defined in the paper of Chang & Tang (1988) as

$$a_1 = a_1^\sigma + a_1^\pi \qquad (9)$$

$$a_2 = a_2^\sigma + a_2^\pi \qquad (10)$$

with

$$a_1^{\sigma,\pi} = \begin{cases} B_0/(1+\cos^2 2\theta_G) \\ \quad \text{for } \sigma \text{ polarization} \\ B_5 \cos 2\theta_G/(1+\cos^2 2\theta_G) \\ \quad \text{for } \pi \text{ polarization} \end{cases} \qquad (11)$$

$$a_2^{\sigma,\pi} = \begin{cases} (B_0^2+B_3^2)/(1+\cos^2 2\theta_G) \\ \quad \text{for } \sigma \text{ polarization} \\ (B_4^2+B_5^2)/(1+\cos^2 2\theta_G) \\ \quad \text{for } \pi \text{ polarization} \end{cases} \qquad (12)$$

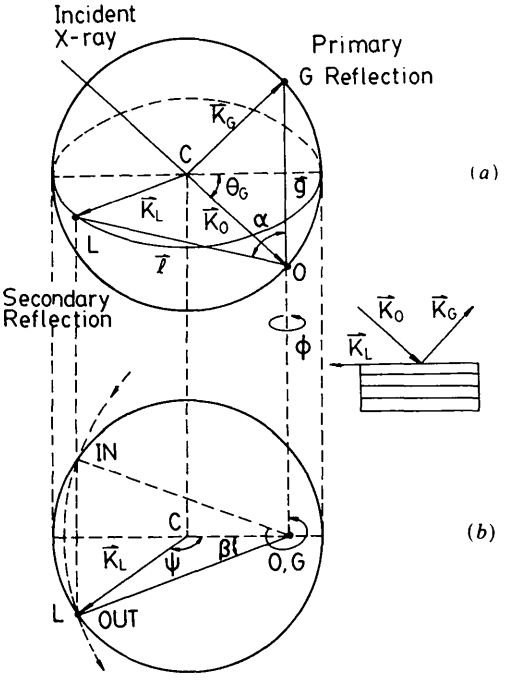

Fig. 1. Geometry of three-beam Bragg-surface diffraction in reciprocal space: (*a*) overview; (*b*) top view. The inset represents the diffraction in real space.

where

$$B_0 = 1-(l/k)^2 \sin^2\alpha \sin^2\beta$$

$$B_3 = (l/k)\sin\alpha\sin\beta\,[(l/k)\sin\alpha\cos\beta\sin\theta_G + (l/k)\cos\alpha\cos\theta_G - \sin 2\theta_G]$$

$$B_4 = (l/k)^2(\cos\alpha\cos\theta_G - \sin\alpha\cos\beta\sin\theta_G)\sin\alpha\sin\beta$$

$$B_5 = \cos 2\theta_G - B_3B_4/[(l/k)\sin\alpha\sin\beta]^2.$$

The phase angle of the structure-factor triplet $F_{G-L}F_LF_{-G}$ is δ. The quantity k/W is the Lorentz factor, where $k = 1/\lambda$.

By considering the mosaic spread η_M of the crystal and the instrumental broadening η_B, we see that the convoluted kinematical intensity distribution takes the form

$$I_k = \frac{a_2\eta_i\eta_T(\Gamma|F_{G-L}||F_L|/|F_GF_O|)^2}{(\Delta\varphi)^2+(\eta_T/2)^2}, \qquad (13)$$

where the total peak width $\eta_T = \eta_i+\eta_B+\eta_M$.

According to (1), (2), (3) and (13), for two given three-beam cases, case A with $\delta>0$ and case B with $\delta<0$, the relative intensity $I'_G(A)$ of case A at $\Delta\varphi=0$ decreases from $I_K(A)$ by the amount $|I_d(A)|$, while $I'_G(B)$ of case B increases from $I_k(B)$ by the amount $|I_d(B)|$. This difference is due mainly to the different signs of δ. If we normalize the experimental intensities $I'_{G,E}(A)$ and $I'_{G,E}(B)$ with the calculated intensities $I'_{G,T}(A)$ and $I'_{G,T}(B)$ of (1), we obtain

$$I'_{G,E}(A)/I'_{G,T}(A)\big|_{\delta>0}^{\Delta\varphi=0} < I'_{G,E}(B)/I'_{G,T}(B)\big|_{\delta>0}^{\Delta\varphi=0}. \qquad (14)$$

Consequently, this leads to the discrimination of the enantiomorph.

If the three-beam diffraction (O, G, L) involves a surface reflection L, difficulty in establishing the relation (14) results. This is because, in this case, the reciprocal-lattice point L lies on the equator of the Ewald sphere (see Fig. 1*a* and the inset). That is, $\gamma_L=0$, $G_2=0$, and $\eta_i=0$. This implies that the convoluted I_k goes to infinity at $\Delta\varphi=0$. An intrinsic peak width of zero is physically meaningless. According to Chang & Tang (1988), η_i in (6) has been derived on the basis of the first-order approximation of the quantity $\mathbf{K}_L\cdot\mathbf{K}_L$ in terms of the accommodation ζ. To overcome this difficulty of having $\eta_i=0$, the second-order terms of ζ in $\mathbf{K}_L\cdot\mathbf{K}_L$ need to be considered in deriving η_i.

From Fig. 1, the wavevector $\mathbf{K}_L$ of the L reflection inside the crystal can be expressed in the following vector form:

$$\mathbf{K}_L = \hat{\mathbf{i}}_x[k\cos\theta_G\sin\beta + k(\Delta\varphi)\cos\theta_G\cos\beta] + \hat{\mathbf{i}}_y(k\gamma_L+k\zeta) + \hat{\mathbf{i}}_z[k\sin\alpha - k\cos\theta_G\cos\beta - k(\Delta\varphi)\cos\theta_G\sin\beta] \qquad (15)$$

where $\hat{\mathbf{i}}_x$ is normal to the plane containing the points O, T and L; $\hat{\mathbf{i}}_y$ is perpendicular to the crystal surface. In connection with the real part ζ' and the imaginary part ζ'' of ζ, the scalar product $\mathbf{K}\cdot\mathbf{K}_L$ can be written as

$$K_L^2 = k^2 - 2W(\Delta\varphi) + k^2(\Delta\varphi)^2\cos^2\theta_G + k^2(\zeta'^2-\zeta''^2) + i2k^2\zeta'\zeta''. \qquad (16)$$

The corresponding resonance failure ξ_L then takes the form

$$2\xi_L = (K^2-K_L^2)/k^2 = \chi_0 + 2W(\Delta\varphi)/k^2 - (\Delta\varphi)^2\cos^2\theta_G - (\zeta'^2-\zeta''^2) - i2\zeta'\zeta'', \qquad (17)$$

where

$$\zeta' = (1/8\gamma_0)[a|\chi_L|^2 - a'|\chi_{L-G}|^2] \qquad (18a)$$

$$\zeta'' = |\chi_0|/(2\gamma_0) \qquad (18b)$$

$$K = k(1+|\chi_0|/2), \qquad (19)$$

according to Chang & Tang (1988). The parameters a and a' are defined, referring to Chang (1984), as

$$a = p_0/\xi_L, \qquad a' = p'_0/\xi_L, \qquad (20)$$

where

$$p_0 = (\hat{\boldsymbol{\sigma}}_O\cdot\hat{\boldsymbol{\sigma}}_L)^2 = \cos^2\beta \qquad (21)$$

$$p'_0 = (\hat{\boldsymbol{\sigma}}_G\cdot\hat{\boldsymbol{\sigma}}_L)^2 = \cos^2\beta \qquad (22)$$

for σ polarization, and

$$p_0 = (\hat{\boldsymbol{\pi}}_O\cdot\hat{\boldsymbol{\sigma}}_L)^2 + (\hat{\boldsymbol{\pi}}_O\cdot\hat{\boldsymbol{\pi}}_L)^2 = 1 \qquad (23)$$

$$p'_0 = (\hat{\boldsymbol{\pi}}_G\cdot\hat{\boldsymbol{\sigma}}_L)^2 + (\hat{\boldsymbol{\pi}}_G\cdot\hat{\boldsymbol{\pi}}_L)^2 = 1-\cos^2\beta\sin^2 2\theta_G, \qquad (24)$$

for π polarization. The polarization unit vectors $\hat{\boldsymbol{\sigma}}$'s and $\hat{\boldsymbol{\pi}}$'s of the reflections involved are defined in Fig. 2. At the kinematical peak position ($\Delta\varphi=0$), the real part $\mathrm{Re}\,[K^2-K_L^2]$ is equal to 0. This means that at

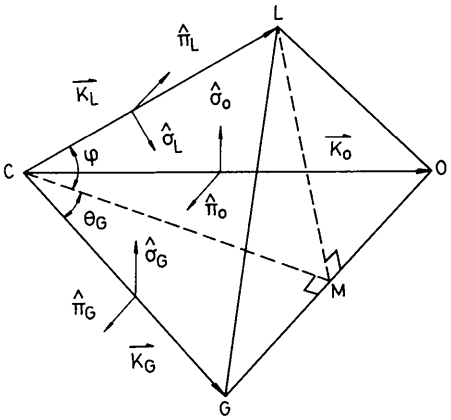

Fig. 2. Definition of the unit vectors of polarization. All $\hat{\boldsymbol{\pi}}$'s are parallel to the OCG plane and the $\hat{\boldsymbol{\sigma}}$'s satisfy $\hat{\boldsymbol{\sigma}}_M\times\hat{\boldsymbol{\pi}}_M=\hat{\mathbf{K}}_M$ for $M=O$, G and L.

$\Delta\varphi = 0$,

$$|2\xi_L| = |I_m(2\xi_L)| = 2|\zeta'\zeta''| = |\chi_0|/(8\gamma_0^2|\xi_L|)[p_0|\chi_L|^2 - p_0'|\chi_{L-G}|^2]. \quad (25)$$

The solution for ξ_L is

$$|\xi_L| = (|\chi_O|^{1/2}/4\gamma_0)[p_0|\chi_L|^2 - p_0'|\chi_{L-G}|^2]^{1/2}. \quad (26)$$

Consequently, the intrinsic peak width η_i becomes

$$\eta_i^\sigma = |[K^2|\chi_O|^{1/2}/(2\gamma_0 W)] \cos\beta \, ||\chi_L|^2 - |\chi_{L-G}|^2|^{1/2}| \quad (27)$$

for σ-polarized wavefields, and

$$\eta_i^\pi = |[K^2|\chi_O|^{1/2}/(2\gamma_0 W)]||\chi_L|^2 - |\chi_{L-G}|^2|^{1/2}| \quad (28)$$

for π-polarized wavefields.

The kinematical intensities at $\Delta\varphi = 0$ for σ- and π-polarized wavefields, according to (13), are

$$I_K^{\sigma,\pi} = 4a_2^{\sigma,\pi}(\eta_i^{\sigma,\pi}/\eta_T)(\Gamma|F_{G-L}||F_L|/|F_G||F_O|)^2. \quad (29)$$

The resultant kinematical intensity $I_{k,T}$ is then equal to

$$I_{k,T} = I_k^\sigma + I_k^\pi. \quad (30)$$

Equation (30) can therefore be used for intensity normalization.

3. Experimental

Bragg-surface three-beam diffraction profiles were obtained for the GaAs 200 reflection and Cu $K\beta$ radiation using the experimental set up described by Tang & Chang (1988). The sample is a plate-like GaAs single crystal with the large flat surface parallel to the (200) atomic planes. Since the primary reflection is 200, all the reflections with the Miller index $h = 1$ are possible surface reflections. Fig. 3 shows the relative positions of the reflections {111}, {113} and {133} on the equatorial plane, with respect to the [100] direction. There are four {111}, eight {113} and four {133} three-beam cases. Owing to the two positions, IN and OUT (see Fig. 1*b*), for each three-beam diffraction during a 360° azimuthal rotation, the number of diffraction cases is doubled. Measurements on peak intensities $I_P = I_G'(\Delta\varphi = 0)$ and full-width η_T at half maximum were made for all the three-beam reflections mentioned above. In order to minimize the errors due to the possible distortion of the Ewald sphere caused by the nonuniformity in dispersion of the incident beam, the data were averaged over each IN-OUT pair. Table 1 lists the peak positions φ, the peak intensities I_P, the widths η_T, the averaged experimental $\bar{I}_{k,E}$, the calculated intensities $I_{k,T}$, the ratio $\bar{I}_{k,E}/I_{k,T}$, and the calculated phase angle δ. The intensity ratio $\bar{I}_{k,E}/I_{k,T}$ *versus* $2a_1/a_2P$, the quantity proportional to I_d/I_k, is plotted in Fig. 4; the average values of $\bar{I}_{k,E}/I_{k,T}$ are indicated by the horizontal lines.

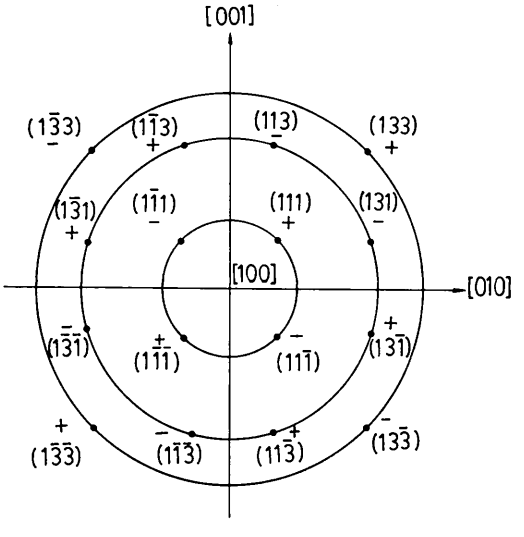

Fig. 3. Relative positions of the reciprocal-lattice points of {111}, {113} and {133} for possible three-beam Bragg-surface diffractions. The signs of δ are also indicated.

4. Results and discussions

According to (14), a comparison between the normalized intensities should, in principle, lead to the discrimination of the enantiomorph. This is actually the case for the {111} and {133} three-beam diffractions. As can be seen in Figs. 4(*a*) and (*c*), the horizontal

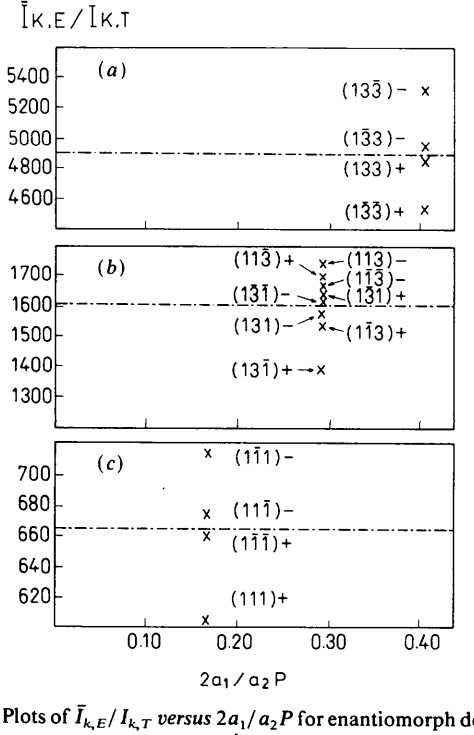

Fig. 4. Plots of $\bar{I}_{k,E}/I_{k,T}$ *versus* $2a_1/a_2P$ for enantiomorph determination.

Table 1. *Summary of the measurements and related calculations ($\varphi = 0$ corresponds to the position where [001] coincides with the plane of incidence*; I: IN, O: OUT *position*)

L	φ(°)	I_P	η_T (0·01°)	$\bar{I}_{k,E}$	$I_{k,T}(\times 10^{-4})$	$\bar{I}_{k,E}/I_{k,T}$	δ(°)
$1\bar{1}1$	39·85 (I)	16·11	3·26	16·17	225·5	717	−76
	230·15 (O)	16·22	3·33				
$11\bar{1}$	219·85 (I)	14·87	3·39	15·02	222·1	676	−76
	50·15 (O)	15·16	3·31				
$1\bar{1}\bar{1}$	309·85 (I)	15·66	3·43	14·37	217·3	661	96
	140·15 (O)	13·08	3·54				
111	129·85 (I)	13·06	3·40	12·96	214·3	605	96
	320·15 (O)	12·85	3·68				
113	87·24 (I)	2·96	3·61	2·96	169·7	1744	−74
	309·63 (O)	2·49	4·21				
$11\bar{3}$	230·37 (I)	3·55	3·59	2·51	149·94	1680	97
	92·76 (O)	2·52	4·18				
$1\bar{1}\bar{1}$	267·24 (I)	3·00	3·40	3·00	18·02	1665	−74
	129·63 (O)	2·54	4·36				
$1\bar{3}\bar{1}$	320·37 (I)	2·57	3·50	2·50	15·39	1624	−74
	182·76 (O)	2·50	3·98				
$1\bar{3}1$	357·24 (I)	2·99	3·40	2·99	18·37	1628	97
	219·63 (O)	3·27	4·22				
131	140·37 (I)	3·17	3·67	2·48	15·63	1587	−74
	2·76 (O)	2·48	3·92				
$1\bar{1}3$	50·37 (I)	3·20	3·39	2·35	15·34	1531	97
	272·76 (O)	2·35	4·07				
$13\bar{1}$	177·24 (I)	2·64	3·28	2·64	19·04	1387	97
	39·63 (O)	3·17	4·29				
$13\bar{3}$	194·40 (I)	1·06	3·93	1·06	1·993	5319	−70
	75·60 (O)	1·06	4·66				
$1\bar{3}3$	14·40 (I)	1·16	3·68	1·02	2·050	4976	−70
	255·60 (O)	0·88	4·67				
133	104·40 (I)	1·08	3·89	0·99	2·049	4832	94
	345·60 (O)	0·90	4·58				
$1\bar{3}\bar{3}$	284·40 (I)	1·04	3·94	0·94	2·049	4588	94
	165·60 (O)	0·83	4·54				

The values of $2a_1/a_2P$ are 0·166, 0·291, and 0·401 for {111}, {113} and {133}, respectively.

lines at the average values of $\bar{I}_{k,E}/I_{k,T}$ separate unambiguously the three-beam diffractions with $\delta < 0$ from those with $\delta > 0$. This separation is, however, not very clear in the {113} case. In Fig. 4(*b*), there are three reflections, $11\bar{3}$, 131 and $1\bar{3}1$, having incorrect signs in δ. This is probably due to the fact that one of each IN–OUT pair of this {113} reflection is close to the peak position of a {111} reflection so that the {113} intensity is affected considerably.

In the theoretical considerations given above, it is interesting to note that, in Bragg-surface three-beam diffraction cases, the intrinsic peak width is nominally proportional to $\chi^{3/2}$ while in Bragg–Bragg and Bragg–Laue cases, referring to Chang & Tang (1988), η_i is a function of χ. Moreover, according to (27) and (28), for particular Bragg-surface diffractions, like the cases discussed above, with $|\chi_L| = |\chi_{L-G}|$, the σ-polarized wavefields affect the η_i value very little. Thus the π-polarized wavefields are the main contributors to the intrinsic peak width. All these points are the consequence of the approximation $\mathrm{Re}\,[K^2 - K_L^2] = 0$, used in the derivation. More precisely, it should be read that $\mathrm{Re}\,[K^2 - K_L^2]$ approaches a minimum value. Improvement on the theory can be made by looking for a better approximation for $\mathrm{Re}\,[K^2 - K_L^2]$.

In conclusion, we have derived the expressions, (27) and (28), for the intrinsic peak width of three-beam Bragg-surface diffraction. With these expressions, the kinematical intensity can easily be calculated. Experimentally, we have demonstrated that the measured peak intensities normalized by the calculated intensities lead to direct determination of the enantiomorph. Utilization of this particular Bragg-surface diffraction peak for enantiomorph discrimination certainly amplifies the applicability of the X-ray multiple diffraction technique for phase determination.

The authors are indebted to the National Science Council for financial support. SSC and MTT are also grateful to the same organization for providing graduate fellowships.

References

CHANG, S. L. (1981). *Appl. Phys.* A**26**, 221–226.
CHANG, S. L. (1982). *Phys. Rev. Lett.* **48**, 163–166.
CHANG, S. L. (1984). *Multiple Diffraction of X-rays in Crystals*, p. 134, Berlin: Springer-Verlag.
CHANG, S. L. (1986). *Phys. Rev. B*, **33**, 5848–5850.
CHANG, S. L. (1987). *Crystallogr. Rev.* **1**, 85–190.
CHANG, S. L. & TANG, M. T. (1988). *Acta Cryst.* A**44**, 1065–1072.
CHAPMAN, L. D., YODER, D. R. & COLELLA, R. (1981). *Phys. Rev. Lett.* **46**, 1578–1581.

COLELLA, R. (1974). *Acta Cryst.* A**30**, 413-423.
EWALD, P. P. & HENO, Y. (1968). *Acta Cryst.* A**24**, 5-15.
HART, M. & LANG, A. R. (1961). *Phys. Rev. Lett.* **7**, 120-121.
HØIER, R. & AANESTAD, A. (1981). *Acta Cryst.* A**37**, 787-794.
HØIER, R. & MARTHINSEN, K. (1983). *Acta Cryst.* A**39**, 854-860.
HÜMMER, K. & BILLY, H. W. (1982). *Acta Cryst.* A**38**, 841-848.
HÜMMER, K. & BILLY, H. W. (1986). *Acta Cryst.* A**42**, 127-133.
HÜMMER, K., WECKERT, E. & BONDZA, H. (1989). *Acta Cryst.* A**45**, 182-187.
JAGODZINSKI, H. (1980). *Acta Cryst.* A**36**, 104-116.
JURETSCHKE, H. J. (1982*a*). *Phys. Rev. Lett.* **48**, 1487-1489.
JURETSCHKE, H. J. (1982*b*). *Phys. Lett.* **92**A, 183-185.
LADD, M. F. C. & PALMER, R. A. (1980). Editors. *Theory and Practice of Direct Methods in Crystallography*, p. 23. New York: Plenum Press.
LIPSCOMB, W. N. (1949). *Acta Cryst.* **2**, 193-194.
MO, F., HAUBACH, B. C. & THORKILDSEN, G. (1988). *Acta Chem. Scand. Ser. A*, **42**, 130-138.
POST, B. (1977). *Phys. Rev. Lett.* **39**, 760-763.
POST, B., NICOLOSI, J. & LADELL, J. (1984). *Acta Cryst.* A**40**, 684-688.
SHEN, Q. (1986). *Acta Cryst.* A**42**, 525-533.
SHEN, Q. & COLELLA, R. (1988). *Acta Cryst.* A**44**, 17-21.
TANG, M. T. & CHANG, S. L. (1988). *Acta Cryst.* A**44**, 1073-1078.
THORKILDSEN, G. (1987). *Acta Cryst.* A**43**, 361-369.

Acta Cryst. (1989). A**45**, 708-715

The Pulsed-Neutron Diffraction Method of Studying Acoustic Phonons in Barium Fluoride and Calcium Fluoride

BY C. J. CARLILE

*Rutherford Appleton Laboratory, Chilton, Didcot, Oxon OX*11 0*QX, England*

AND B. T. M. WILLIS

Chemical Crystallography Laboratory, 9 *Parks Road, Oxford OX*1 3*PD, England*

(*Received* 22 *March* 1989; *accepted* 17 *May* 1989)

Abstract

Earlier papers [Willis (1986). *Acta Cryst.* A**42**, 514-525; Schofield & Willis (1987). *Acta Cryst.* A**43**, 803-809] have discussed the nature of the thermal diffuse scattering (TDS) arising from the interaction of a 'white' beam of thermal neutrons with the acoustic modes of vibration in a single crystal. A simpler version of the scattering theory is now given which does not have recourse to the numerous equations employed in previous treatments. The theory is applied to the interpretation of TDS data from BaF_2 and CaF_2 to give the velocity of sound in these crystals as a function of the direction of propagation.

1. Introduction

This paper is concerned with the scattering of pulsed neutrons, where each pulse contains a wide band of neutron wavelengths, by acoustic phonons in a single crystal. The theoretical treatment for *monochromatic* neutrons, scattered by phonons through a *variable* angle, has been covered by Seeger & Teller (1942), Waller & Froman (1952) and Lowde (1954). The pulsed neutron case, dealing with a *white* beam of neutrons scattered at a *fixed* angle, has unusual features which do not occur in the monochromatic case. These features give rise to the possibility of carrying out novel inelastic experiments, as we shall describe later.

The main features of the scattering theory for pulsed neutrons have been described by Willis (1986) and by Schofield & Willis (1987). For slower-than-sound neutrons, scattered at a fixed angle close to 180° (*i.e.* in back scattering), there is a wavelength window in the incident beam for which thermal diffuse scattering is forbidden. One edge of the window is associated with the absorption of acoustic phonons, and the other edge with their emission. By measuring the cut-off wavelengths for different angles of offset from the Bragg position, it is possible to determine the velocity of these acoustic phonons as a function of their direction of propagation. Earlier results from pyrolytic graphite have been given by Willis, Carlile, Ward, David & Johnson (1986).

In the next section we show how the principal results of the scattering theory can be derived using simple geometrical arguments alone. It is assumed that the crystal is elastically isotropic, whereas all crystals (including cubic crystals) are elastically anisotropic. For this reason the analysis is extended in §3 to the anisotropic case. Experimental results on the isomorphous crystals barium fluoride and calcium fluoride, which have different degrees of elastic anisotropy, are presented in § 4.

0108-7673/89/100708-08$03.00